

# CHEMISTRY

## A European Journal

A Journal of



### Accepted Article

**Title:** Dynamic Coordination Chemistry of Fluorinated Zr-MOFs:  
Synthetic Control and Reassembly/Disassembly beyond de novo  
Synthesis to Tune the Structure and Property

**Authors:** Cheng-Xia Chen, Yan-Zhong Fan, Chen-Chen Cao, Hai-Ping  
Wang, Ya-Nan Fan, Ji-Jun Jiang, Zhang-Wen Wei, Guillaume  
Maurin, and Cheng-Yong Su

This manuscript has been accepted after peer review and appears as an Accepted Article online prior to editing, proofing, and formal publication of the final Version of Record (VoR). This work is currently citable by using the Digital Object Identifier (DOI) given below. The VoR will be published online in Early View as soon as possible and may be different to this Accepted Article as a result of editing. Readers should obtain the VoR from the journal website shown below when it is published to ensure accuracy of information. The authors are responsible for the content of this Accepted Article.

**To be cited as:** *Chem. Eur. J.* 10.1002/chem.202001052

**Link to VoR:** <http://dx.doi.org/10.1002/chem.202001052>

Supported by  
**ACES**

WILEY-VCH

# Dynamic Coordination Chemistry of Fluorinated Zr-MOFs: Synthetic Control and Reassembly/Disassembly beyond *de novo* Synthesis to Tune the Structure and Property

Cheng-Xia Chen<sup>[a]</sup>, Yan-Zhong Fan<sup>[a]</sup>, Chen-Chen Cao<sup>[a]</sup>, Hai-Ping Wang<sup>[a]</sup>, Ya-Nan Fan<sup>[a]</sup>, Ji-Jun Jiang<sup>[a]</sup>, Zhang-Wen Wei<sup>\*[a]</sup>, Guillaume Maurin<sup>\*[b]</sup>, and Cheng-Yong Su<sup>\*[a][c]</sup>

**Abstract:** Known for excellent stability, porosity and functionality, the high-valent Zr<sup>4+</sup> metal-organic frameworks (Zr-MOFs) still meets synthetic challenge in modulating the strength of Zr-O<sub>carboxylate</sub> linkage. Herein we explore the unusual coordination dynamics of fluorinated Zr-MOFs by designing two trifluoromethyl modified ligands with distinct geometry preference to form a family of thermodynamic and kinetic products. The low-connecting kinetic Zr-MOFs possess substitutable coordination sites to endow Zr<sub>6</sub>-cluster with extra dynamic behaviors, thus opening a post-synthetic pathway to sequential reassembly/disassembly processes. Comprehensive factors, including ligand geometry, Zr<sub>6</sub>-cluster connectivity, acid modulator and reaction temperature/concentration, have been studied for controllable syntheses. The stability, hydrophobicity and gas adsorption/separation properties of obtained Zr-MOFs are explored. This work sheds light on the understanding of the dynamic coordination chemistry of Zr-MOFs beyond strong Zr-O bond, which poses a versatile platform for modification and functionalization of Zr-MOFs.

## Introduction

In the past decades, metal-organic frameworks (MOFs) have attracted a lot of attention as an emerging class of modular porous materials for their potential applications in many areas, including gas storage,<sup>[1]</sup> separation<sup>[2]</sup> and catalysis<sup>[3]</sup>, owing to their designable topology, permanent porosity, high surface area and tunable functionality.<sup>[4]</sup> Among them, Zr-MOFs based on strong Zr-O<sub>carboxylate</sub> bonds<sup>[5]</sup> or F-MOFs constructed with fluorinated ligands<sup>[6]</sup> have been intensively studied for the sake of high thermal and chemical stability which could enable more practical applications.<sup>[5a, 6b, 7]</sup> Moreover, F-MOFs with fluorine-decorated channels are expected to exhibit high gas affinity, enhanced hydrophobicity, lower surface energy and surface tension, as well as excellent optical and electrical properties.<sup>[6a, 6c, 8]</sup> Following our early endeavor to construct highly stable F-MOFs<sup>[9]</sup> for water sensing,<sup>[10]</sup> crystalline sponge<sup>[11]</sup> and gas

adsorption,<sup>[12]</sup> we are devoting to combine both attributes from Zr-MOFs and F-MOFs to design fluorinated Zr-MOFs.<sup>[12-13]</sup> The conventional paradigm is that the strong Zr-O bond is responsible for the ultra-high stability of Zr-MOFs. However, recent studies revealed that Zr-O bond is also dynamic and can undergo dissociation and association processes under suitable conditions.<sup>[14]</sup> In this scenario, the terminal OH/H<sub>2</sub>O groups coordinating to Zr<sup>4+</sup>-centers in the kinetic Zr-MOFs of lower connectivity can be replaced by carboxylate groups of secondary or tertiary linkers to transform into higher connecting products.<sup>[15]</sup> As proposed by Zhou<sup>[16]</sup> and further supported by the calculations of Vandichel et al,<sup>[17]</sup> installation of auxiliary ligands onto Zr<sub>6</sub>-clusters is a highly exothermic process. So Zr-MOFs with 12-connected Zr<sub>6</sub>-clusters, *i.e.* saturated clusters, have low energy state and are thermodynamically favored. On the other hand, kinetic products having low-connected Zr<sub>6</sub>-clusters, *i.e.* unsaturated clusters, can act as intermediates for further ligand installation and even uninstallation,<sup>[12, 15b, 18]</sup> which offers a versatile platform to create multivariate MOFs (MTV-MOFs) and tune their functionality. Such unusual coordination dynamics enriches the chemistry of post-syntheses<sup>[19]</sup> to allow disassembly and re-assembly of Zr-MOFs for multi-functionality, *e.g.*, swing the roles of primary Zr-MOFs for multi-purpose gas adsorption,<sup>[15b]</sup> catalysis<sup>[18]</sup> and fluorescence.<sup>[20]</sup>

In this paper, we present a comprehensive study on dynamic nature of Zr-O bonds with respect to control of thermodynamic or kinetic Zr-MOF products, endowing a rich strategy to guide syntheses of MTV-Zr-MOFs with 8-, 10- and 12-connectivities and tunable functions (Figure 1). Thermodynamic and kinetic factors relevant to intermediate energy level, cluster connectivity, ligand conformation, reaction temperature and acid modulator have been systematically studied by design of two comparable fluorinated ligands **H<sub>2</sub>L<sup>1</sup>/H<sub>2</sub>L<sup>2</sup>** (**H<sub>2</sub>L<sup>1</sup>** = 2,2'-bis(trifluoromethyl)-[1,1'-biphenyl]-4,4'-dicarboxylate; **H<sub>2</sub>L<sup>2</sup>** = 3,3'-bis(trifluoromethyl)-[1,1'-biphenyl]-4,4'-dicarboxylate) with distinguishable steric hindrance of trifluoromethyl (-CF<sub>3</sub>) groups. Seven fluorinated Zr-MOFs, *i.e.*, LIFM-28lp (lp means large-pore), LIFM-28np (np means narrow pore), LIFM-34a, LIFM-34b, LIFM-35, LIFM-36 and LIFM-86 (LIFM: Lehn Institute of Functional Materials) are constructed *via de novo* synthesis or sequential dynamic spacer installation of secondary/tertiary ligands **H<sub>2</sub>L<sup>1</sup>** and **H<sub>2</sub>L<sup>3</sup>** (**H<sub>2</sub>L<sup>3</sup>** = 2',5'-difluoro-[1,1':4',1''-terphenyl]-4,4''-dicarboxylate).<sup>[15b]</sup> This offers a unique scenario to obtain fluorinated Zr-MOFs with finely tuned structure and F-distribution benefiting stability, hydrophobicity and gas adsorption. Water vapor adsorption demonstrates that the protection of the hydrophilic Zr<sub>6</sub>-clusters by fluorinated groups can dramatically increase the MOF hydrophobicity. Gas adsorption studies further confirm that introduction of fluorinated groups with varied densities and different positions provide effective ways to

[a] Dr. C.-X. Chen, Y.-Z. Fan, C.-C. Cao, Dr. H.-P. Wang, Y.-N. Fan, Dr. J.-J. Jiang, Dr. Z.-W. Wei, Prof. C.-Y. Su  
MOE Laboratory of Bioinorganic and Synthetic Chemistry, Lehn Institute of Functional Materials, School of Chemistry  
Sun Yat-Sen University  
Guangzhou 510275, China  
E-mail: cecssy@mail.sysu.edu.cn; weizhw3@mail.sysu.edu.cn

[b] Prof. G. Maurin  
Institut Charles Gerhardt Montpellier UMR 5253 CNRS  
Université de Montpellier  
Place E. Bataillon, 34095 Montpellier Cedex 05, France  
E-mail: Guillaume.Maurin@univ-montp2.fr

[c] Prof. C.-Y. Su  
State Key Laboratory of Applied Organic Chemistry  
Lanzhou University  
Lanzhou 730000, China

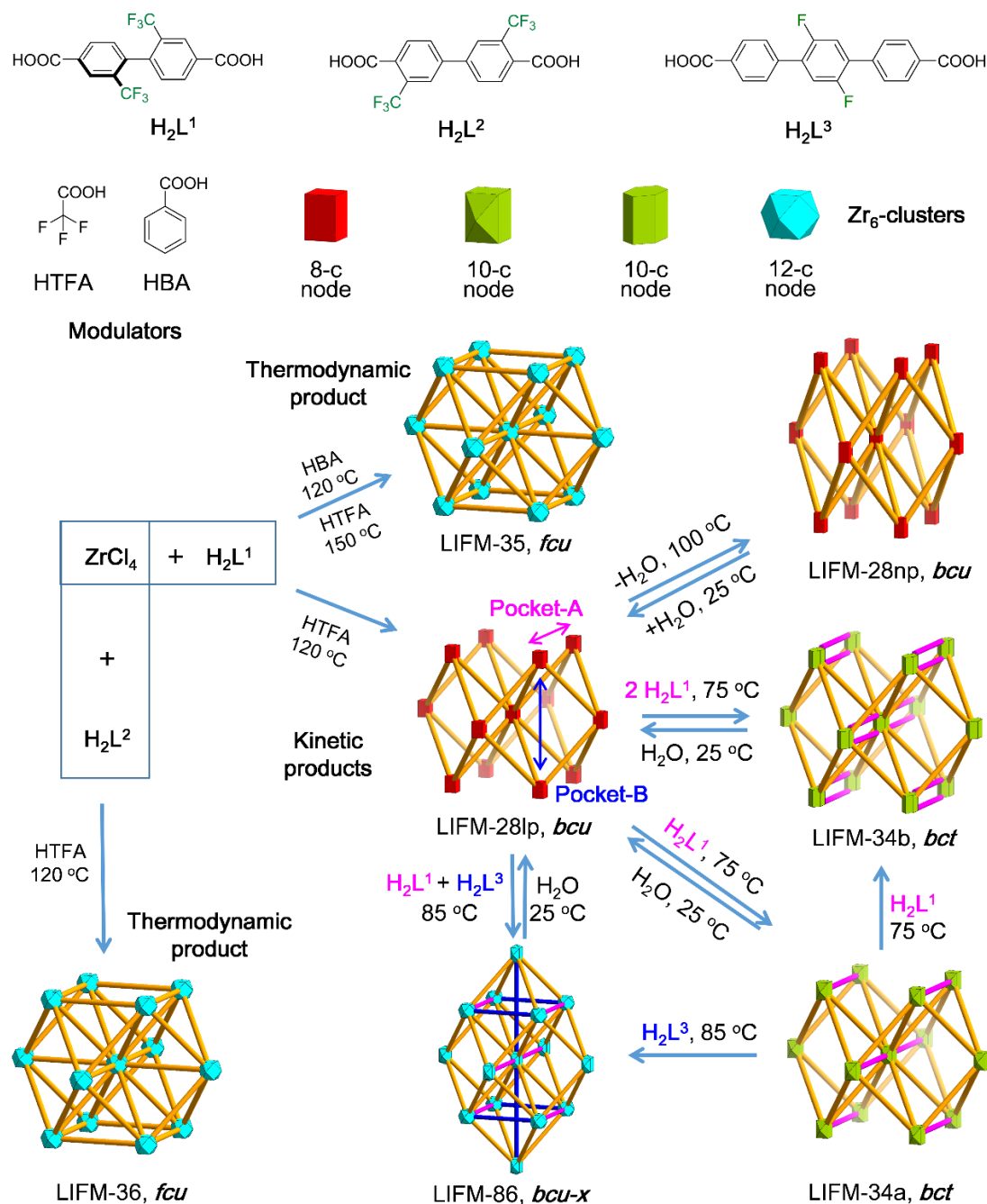


**Figure 1.** A family of Zr-MOFs (LIFM-28lp, LIFM-28np, LIFM-34a, LIFM-34b, LIFM-35, LIFM-36 and LIFM-86) demonstrating synthetic control of thermodynamic and kinetic products and structural transformations.

enhance the CO<sub>2</sub> and R22 capture capacity and tune gas separation ability.

## Results and Discussion

**Synthetic map and geometric origin of coordination dynamics.** It is well known that reaction of BPDC (4,4'-biphenyldicarboxylate) linear ligand and Zr<sup>4+</sup> oxo-cluster produces UiO-67 prototype MOF having 12-connecting Zr<sub>6</sub>-cluster, which is the thermodynamic product.<sup>[21]</sup> When introducing steric groups to BPDC, the kinetic product with low

8-connectivity is expected to be more favored.<sup>[12, 15a]</sup> To further explore if the thermodynamic and kinetic products can be modulated by introducing steric groups onto different positions, we designed two fluorinated BPDC ligands,  $H_2L^1$  and  $H_2L^2$ , with -CF<sub>3</sub> groups on 2,2'- or 3,3'-positions respectively, and obtained a series of fluorinated Zr-MOFs with distinct physicochemical attributes (Figures 1, S1-S9 and Table S1). Reaction of  $H_2L^2$  with ZrCl<sub>4</sub> in DMF (*N,N*-dimethylformamide) in the presence of trifluoroacetic acid (HTFA) modulator at 120 °C afforded LIFM-36. Single crystal X-ray structural analysis indicates that LIFM-36 is isostructural to UiO-67,<sup>[21]</sup> showing *fcu* topology with Zr<sub>6</sub>-clusters as 12-connecting nodes (Figure 1). Therefore, ligand

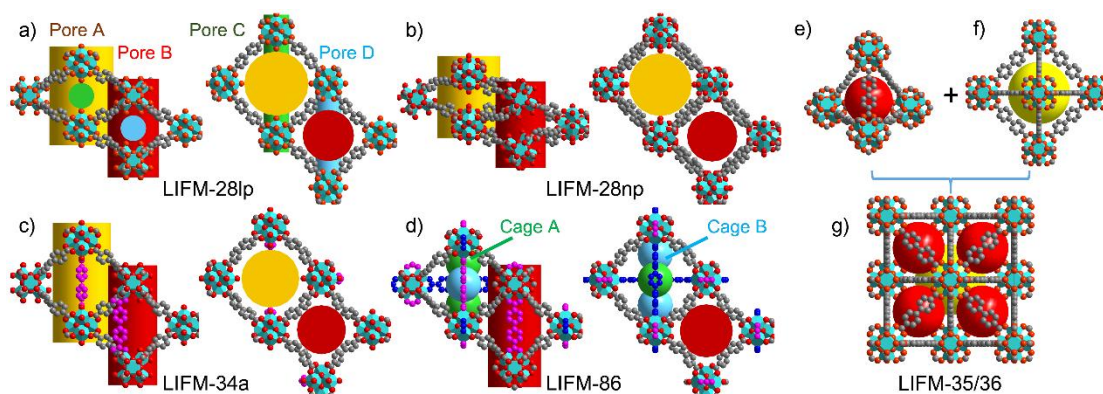


**Figure 2.** Different pores in (a) LIFM-28lp, (b) LIFM-28np, (c) LIFM-34a and (d) LIFM-86. (e) Small tetrahedral cage, (f) large octahedral cage and (g) their packing mode in LIFM-35 and LIFM-36. Color scheme: aqua polyhedra, Zr; red, O; grey, C; pink, inserted  $L^1$  ligand; blue, inserted  $L^3$  ligand. All H and  $-CF_3$  groups are omitted for clarity.

$H_2L_2$  prefers to form the thermodynamic product. There are two kinds of polyhedral cages in LIFM-36, *i.e.*, a small tetrahedral cage constructed from four  $Zr_6$ -clusters and six  $L^2$  linkers with a cavity diameter of *c.a.* 12.1 Å, and an octahedral cage consisting of six  $Zr_6$ -clusters and twelve  $L^2$  linkers with a cavity diameter of *c.a.* 15.2 Å (Figure 2). In contrast, reaction of ligand  $H_2L^1$  and  $ZrCl_4$  under the same condition yielded an 8-connecting kinetic product LIFM-28lp, which can transform to narrow pore LIFM-28np by removing solvent molecules while keeping *bcu* topology unchanged (Figures S10-11).<sup>[12]</sup> The corresponding crystal lattice presents four types of pores (Figure 2), where there are two types of pockets that can accommodate additional linkers to connect neighboring  $Zr_6$ -clusters by virtue of replacing terminal  $H_2O$ . As illustrated in Figure 1, installation of one or two  $H_2L^1$  linkers into the so-called Pocket-A creates 10-connecting LIFM-34a and 34b of *bct* topology, respectively. Moreover, installation of  $H_2L^1$  and  $H_2L^3$  into Pocket-A and Pocket-B simultaneously lead to 12-connecting LIFM-86 of *bcu-x* topology. Some pores are blocked by inserted ligands, but more  $-CF_3$  groups are brought into the interior of cavities. It is noticeable that, by elevating the reaction temperature to 150 °C or change the modulator to benzoic acid (HBA), 12-connecting LIFM-35 of *fcu* topology instead of low-connecting LIFM-28 was obtained, which is isostructural to LIFM-36. Therefore, ligand  $H_2L^1$  is able to form both thermodynamic and kinetic products, depending on the modulation of the reaction conditions.

Above results suggest that the location of two  $-CF_3$  groups may significantly affect the ligand conformation, which plays a key role to direct the framework topology and consequent connectivity of the  $Zr_6$ -clusters,<sup>[12, 15b, 22]</sup> thus able to tune the thermodynamic and kinetic products in a predictable and controllable way. As shown in Figure 3, the geometric analysis of the framework topologies reveals that, the *fcu* Zr-MOF requires 12 symmetrically identical linkers with two coplanar  $-COO^-$  groups, while the 8 equivalent linkers in *bcu* Zr-MOF have to be nonplanar<sup>[12, 15a]</sup> or nonlinear.<sup>[23]</sup> Moreover, the 8 unsaturated coordination sites in *bcu* Zr-MOF are located in one equatorial plane, and connections between two pairs of adjacent  $Zr_6$ -clusters need a linker with two  $-COO^-$  groups coplanar. Therefore, the coplanar conformation of two  $-COO^-$  is necessary to form 12-connecting thermodynamic Zr-MOF with linear dicarboxylate linkers, while the nonplanar conformation of two  $-$

$COO^-$  is the prerequisite for the formation of 8-connecting kinetic Zr-MOF. However, further spacer installation to increase the connectivity needs a linker adopting coplanar conformation, which may introduces conformational tension. Such linker geometric difference accounts for the fact that nonplanar dicarboxylate linkers prefer to form 8-connecting kinetic product, since structural transformation to 12-connecting thermodynamic product demands additional activation to surpass energy barrier from coplanar enforcement (see discussion below). Furthermore, because the 8-connecting Zr-cluster itself has neutral charge, the remaining 8 coordination sites may become labile with  $H_2O$  molecules being easily substituted by insertion of additional linkers, which is enthalpically driven to turn into 10- or 12-connecting Zr-MOFs. The lability of these 8 unsaturated Zr-sites may also render facile removal of the inserted linkers, since neutral dicarboxylate linkers are adequate for installation without deprotonation, and release of installed linkers can reduce the framework strain considering the fact that the framework of LIFM-28lp tends to convert to shrunken LIFM-28np *via* removal of  $H_2O$  solvents by heating.<sup>[12]</sup> As a consequence, the kinetic Zr-MOF will be endowed with extra coordination dynamics for post-synthesis in a sequential and reversible way by the framework geometric requirement of distinguishable linkers.

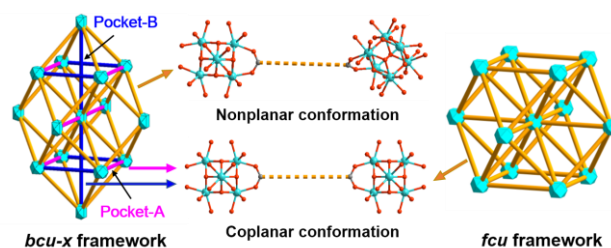


**Figure 3.** Thermodynamic *fcu* Zr-MOF with 12 dicarboxylate linkers identical in coplanar conformation, and kinetic *bcu-x* Zr-MOF characteristic of 8 nonplanar dicarboxylate linkers and insertion of two types of coplanar spacers.

**Control factors for thermodynamic and kinetic products.** Generally speaking, when reaction pathway toward thermodynamic product has a high energy barrier, the reaction may proceed to a direction with lower barrier to produce kinetic

product. Hence modulation of reaction conditions is able to alter reaction pathways to generate different products through regulating the activation energy. We have thoroughly investigated reaction conditions that influence reaction directions.

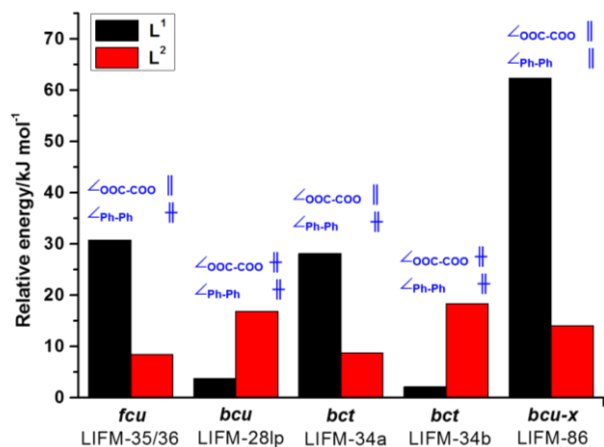


**Figure 4.** The calculated relative energy of  $H_2L^1$  and  $H_2L^2$  adopting coplanar (||) and nonplanar (⊥) conformations of two carboxylate groups ( $\angle_{OOC-COO}$ ) and phenyl rings ( $\angle_{Ph-Ph}$ ) in different Zr-MOFs. See text for more details.

**Ligand geometry.** The ligand  $H_2L^1$  differs from  $H_2L^2$  in the positions of  $-CF_3$  groups on two central phenyl rings, where two  $-CF_3$  groups in adjacent 2,2'-positions have steric hindrance to prevent two phenyl rings from coplanar, while two 3,3'-substituted  $-CF_3$  groups are far apart without remarkable conformation influence. Density functional theory (DFT) calculations were performed on  $H_2L^1$  and  $H_2L^2$  for variable conformations adopted in Zr-MOFs (Figure 4; Table S4), which unveils the geometric reason why  $H_2L^1$  and  $H_2L^2$  produce different Zr-MOFs from the same starting intermediate.<sup>[24]</sup> For LIFM-35/36, enforcement of two  $-COO^-$  groups to be coplanar (dihedral angle of  $\angle_{OOC-COO}$  close to  $0^\circ$ ) leads to a much higher relative energy of  $H_2L^1$  than that of  $H_2L^2$ . On the contrary, for LIFM-28lp, the twisted conformation with both two  $-COOH$  groups and two phenyl rings ( $\angle_{Ph-Ph}$ ) adopting nonplanar orientations is much favored by  $H_2L^1$  than  $H_2L^2$ . Therefore,  $H_2L^1$  is prone to follow a reaction pathway toward kinetic *bcu* Zr-MOFs, while  $H_2L^2$  favors the generation of *fcu* Zr-MOFs dominated by enthalpy gain from 12-connected thermodynamic product. The inserted  $H_2L^1$  in LIFM-34a also adopts a coplanar conformation of two  $-COOH$  groups, which causes relatively high energy, in comparison to LIFM-34b having two  $H_2L^1$  inserted in one Pocket-A with a nonplanar conformation. In LIFM-86, the inserted  $H_2L^1$  adopts a transplanar conformation, displaying very high relative energy that implies intensive strain of the framework. Such relationship between ligand conformations and Zr-MOF topologies presents a predictable design principle of proper ligands to guide the synthesis of desired Zr-MOF structures,<sup>[24]</sup> and a rational explanation of their chemical stability and coordination dynamics (see discussion below).

**Reaction temperature.** To obtain thermodynamic products from  $H_2L^1$ , higher reaction temperature is expected to overcome the energy gap by forcing two carboxylate groups coplanar, which may be compensated by additional enthalpy contribution from connectivity increase. Indeed, a new Zr-MOF named as

LIFM-35 was produced after rising temperature from 120 to 150 °C, which is as effective as the *increasing temperature synthetic strategy* reported by Zhou group.<sup>[22]</sup> It is understandable that conformational strain is generated to disturb ideal crystallization, and single-crystal suitable for X-ray crystallography is hard to obtain. However, the powder X-ray diffraction (PXRD) pattern of LIFM-35 matches well with the pattern of UiO-67 (Figure S7),<sup>[21]</sup> indicating that they are isostructural. So LIFM-35 is a thermodynamic product of  $H_2L^1$  (Figure 1).<sup>[22]</sup> Therefore, temperature plays an essential role to determine the final products of  $H_2L^1$ , which will guide reaction process through either thermodynamically or kinetically driven pathways.

**Modulator.** Acid modulators are known to be crucial in Zr-MOF syntheses for tuning crystal growth speed and product topology. We noticed that, when changing HTFA modulator to HBA during the reaction between  $H_2L^1$  and  $ZrCl_4$  under comparable conditions (Figure 1), LIFM-35 instead of LIFM-28 was obtained, suggesting a *changing modulator approach* to direct reaction pathway toward thermodynamic product. This represents an unprecedented example to obtain *fcu* product from linear dicarboxylate ligand having steric hindrance. It is supposed that HTFA/HBA modulators react with  $Zr^{4+}$  ion firstly to form  $Zr_6$ -TFA/BA precursors serving as initial intermediates in subsequent Zr-MOF growth,<sup>[5a, 25]</sup> although it should be born in mind the mechanism for modulators interacting with the self-assembly process is complicated. Because  $-CF_3$  group is strongly electron withdrawing in contrast to phenyl ring with electron-donating ability, the deprotonated BA<sup>-</sup> is much basic than TFA<sup>-</sup> to form stronger Zr- $O_{BA}$  bond. As a consequence, replacing BA<sup>-</sup> from  $Zr_6$ -BA precursor by dicarboxylate linker needs to climb relatively higher energy barrier to produce Zr-MOF (see discussion below), which prevents formation of kinetic *bcu* Zr-MOF, but facilitates reaction pathway toward *fcu* Zr-MOF driven most probably by enthalpy compensation from four additional Zr- $O_{dicarboxylate}$  bonds. On the contrary, the linker replacement on  $Zr_6$ -TFA is comparatively facile because of lower energy barrier originated in weaker Zr- $O_{TFA}$  bonds, which make the reaction pathways easily influenced by external factors, e.g., temperature, to switch between kinetic or thermodynamic products as mentioned above. These results demonstrate that the modulator also plays a vital role in Zr-MOF syntheses.

**Structural transformation based on dynamic coordination chemistry.** At early stage, Zr-O bond is considered highly inert and irreversible, since growing Zr-MOF single-crystals is generally difficult. However, the finding that acid modulators can facilitate crystal growth and structural tuning actually hinted for its intrinsic dynamic nature according to the competing and substituting mechanism. Our finding that the 8-connecting kinetic *bcu* Zr-MOF features in dynamic spacer installation in a reversible fashion<sup>[12, 15b, 18]</sup> further proves unique coordination dynamics of the unsaturated  $Zr_6$ -cluster derived from geometric origin as discussed above. Such dynamic coordination chemistry of kinetic LIMF-28 allow us to manipulate the structure transformation and create new Zr-MOF topologies that cannot be obtained from *de novo* syntheses.

As seen from Figure 1, when clean LIFM-28lp reacted with one equivalent amount of additional  $H_2L^1$ , LIFM-34a of 10-connecting *bct* topology was obtained with each Pocket-A installed with one secondary  $H_2L^1$  (Figures S12-S14 and S17, Table S2). Using excess amount of  $H_2L^1$  to react with LIFM-28lp,

LIFM-34b was obtained with every Pocket-A installed with two  $\text{H}_2\text{L}^1$  (Figures S12, S15-S16, S18-S20 and Table S3). The single-crystal analyses unveil that, in both cases, the inserted  $\text{H}_2\text{L}^1$  takes a dangle fashion to coordinate with  $\text{Zr}_6$ -cluster through one O atom (Figure S12). This is due to the fact that the inserted  $\text{H}_2\text{L}^1$  has to adopt coplanar conformation for chelating coordination, which is different from the nonplanar ones in LIFM-28lp framework, so bulky  $-\text{CF}_3$  groups disfavours chelating coordination. The inserted linkers can be easily removed by soaking the samples in water, suggesting a reversible installation and uninstallation processes (Figure S14). Moreover, insertion of two  $\text{H}_2\text{L}^1$  can be achieved from either a one-step process, or a successive two-step process, but uninstallation of LIFM-34b is not able to stop at LIFM-34a by removal of just one inserted linker (Figures S16 and S19). Hence, LIFM-34a/LIFM-34b are restored to LIFM-28lp directly in one step (Figure 1). Further insertion of tertiary  $\text{H}_2\text{L}^3$  into LIFM-34a can lead to transformation to 12-connecting LIFM-86 simplified as uninodal **bcu-x** topology,<sup>[15b]</sup> which was also attainable from one-step insertion simultaneously with every Pocket-A accommodating one  $\text{H}_2\text{L}^1$  and every Pocket-B accommodating one  $\text{H}_2\text{L}^3$  (Figure 1, S21). These three Zr-MOFs with distinguishable linkers in framework can only be generated from LIFM-28 in a stepwise manner, *i.e.*, *via* sequential assembly of secondary and tertiary linkers. Since the inserted linkers can be removed, a disassembly process is achievable, demonstrating a rich and reversible post-synthetic approach to create novel MTV Zr-MOFs beyond *de novo* synthesis based on their dynamic coordination chemistry.

DFT calculations were equally performed to estimate the energy differences of reaction activation  $\Delta E$  associated with structural transformations between these different Zr-MOFs (Section S12 in Supporting Information). These computations provide evidence that, from a thermodynamic standpoint, the transformations of LIFM-28lp into LIFM-28np, LIFM-34a, LIFM-34b and LIFM-86 are energetically favored since the energy differences corresponding to transformation reactions are all negative (Eqs. S1-S4 in Supporting Information). The same conclusion holds true for the transformations of LIFM-34a into both LIFM-34b and LIFM-86 (Eqs. S5-S6). Considering the contribution of the entropy, the Gibbs free energy will be even more negative for Eqs. S2-S6 since the corresponding reactions were performed experimentally at high temperature. This whole set of predictions supports all the mentioned transformations experimentally observed. Thus an estimated energy scheme was plotted in Scheme S1, which matches our synthetic map (Figures 1 and 5) very well.

From above discussion we can see that the Zr-O bond is intrinsically dynamic. Through judicious design of dicarboxylate ligand conformations and proper selection of reaction temperature and acid modulators, both thermodynamic and kinetic Zr-MOF products could be obtained. A general synthetic map including possible reaction pathways and relative energy barriers is proposed in Figure 5. In the presence of acid modulators HTFA and HBA, formation of  $\text{Zr}_6$ -TFA/BA precursors is favored through reactions 1 and 2, which serve as beginning intermediates to direct the subsequent Zr-MOF construction. Following reaction pathways 3-7, Zr-MOF products LIFM-28lp, LIFM-35 and LIFM-36 may be generated by preferential exchange of  $\text{Zr-O}_{\text{modulator}}$  bonds with  $\text{Zr-O}_{\text{dicarboxylate}}$  bonds, which is both entropically and enthalpically driven but depends on the

interplay of ligand geometry, temperature and modulator. The coplanar or nonplanar conformations of ligand take the priority to dictate the orientation of  $\text{Zr}_6$ -clusters to be connected, thus guide the framework topology towards 12-connecting **fcu** thermodynamic or 8-connecting **bcu** kinetic products. The stronger basicity and coordination ability of  $\text{BA}^-$  impart lower energy state but higher energy barrier to  $\text{Zr}_6$ -BA precursor, and *vice versa* for  $\text{Zr}_6$ -TFA precursor. Therefore, starting from  $\text{Zr}_6$ -TFA with relatively lower activation energy, either thermodynamic LIFM-36 or kinetic LIFM-28lp can be built from  $\text{H}_2\text{L}^2$  or  $\text{H}_2\text{L}^1$  *via* reactions 7 or 3, respectively, dominated by their favorite coplanar or nonplanar conformations requisite for distinct framework topologies. In contrast, formation of kinetic product from  $\text{Zr}_6$ -BA is not favored because its high energy state prevents transient stay at low-connecting kinetic LIFM-28lp (reaction 4) but prefers giant enthalpic gain from 12-connecting thermodynamic product (reaction 6). This is evident from reaction 5 that, at elevated temperature, the nonplanar  $\text{H}_2\text{L}^1$  can even be enforced to coplanar conformation to convert to thermodynamic LIFM-35 through a higher activation pathway. The dynamic nature of Zr-O bond has been further testified by the observation that, in the presence of excess amount of HBA or HTFA, all Zr-MOF products are dissolved following the reversed reaction pathways and turned back to  $\text{Zr}_6$ -BA or  $\text{Zr}_6$ -TFA precursors (Figure S22).<sup>[19b]</sup>

More dynamic behavior is found for the kinetic LIFM-28lp, of which the unsaturated Zr-cluster possess 8 terminal sites occupied by  $\text{H}_2\text{O}$  molecules.<sup>[12]</sup> Fully reversible installation and uninstallation of the secondary and tertiary ligands proceed *facially via* replacement reactions 9-12 to enable sequential reassembly and disassembly. The installed spacers can be easily uninstalled by simply soaking the Zr-MOF crystals into water at ambient temperature, indicating a reverse shift of insertion reactions by increasing water concentration, and a dynamic Zr-O binding of inserted ligands comparable with that of  $\text{H}_2\text{O}$  coordination. This is reasonable because, once the 8-connecting Zr-clusters are formed, the neutral kinetic product only requires insertion of additional  $\text{H}_2\text{L}^1$  without prerequisite deprotonation. Moreover, insertion of additional linkers causes overall strain energy to expand the 8-connecting framework,<sup>[12]</sup> thus apt to release the inserted linkers to turn back to the favorite shrunken state as mentioned above. The energy barrier and energy difference between LIFM-28lp and LIFM-34a/34b/86 are relatively low, which facilitates reversible installation/uninstallation processes for structural transformations. Such coordination dynamics endows Zr-MOFs with effective and useful design strategies to guide fluorinated Zr-MOF syntheses and tune MOF structures for various functions.

**Structure-property comparison and modulation.** In order to understand specific physicochemical properties of diverse Zr-MOFs in relation with their structural attributes, the thermal and chemical stability, porosity, gas uptake capacity and separation ability have been evaluated. The phase purity of bulk crystalline materials has been individually confirmed by PXRD patterns (Figures S4-S9).

**Thermal and chemical stability.** Thermogravimetric analysis (TGA) and variable-temperature powder X-ray diffraction (VT-PXRD) of all Zr-MOFs were performed to evaluate their thermo-

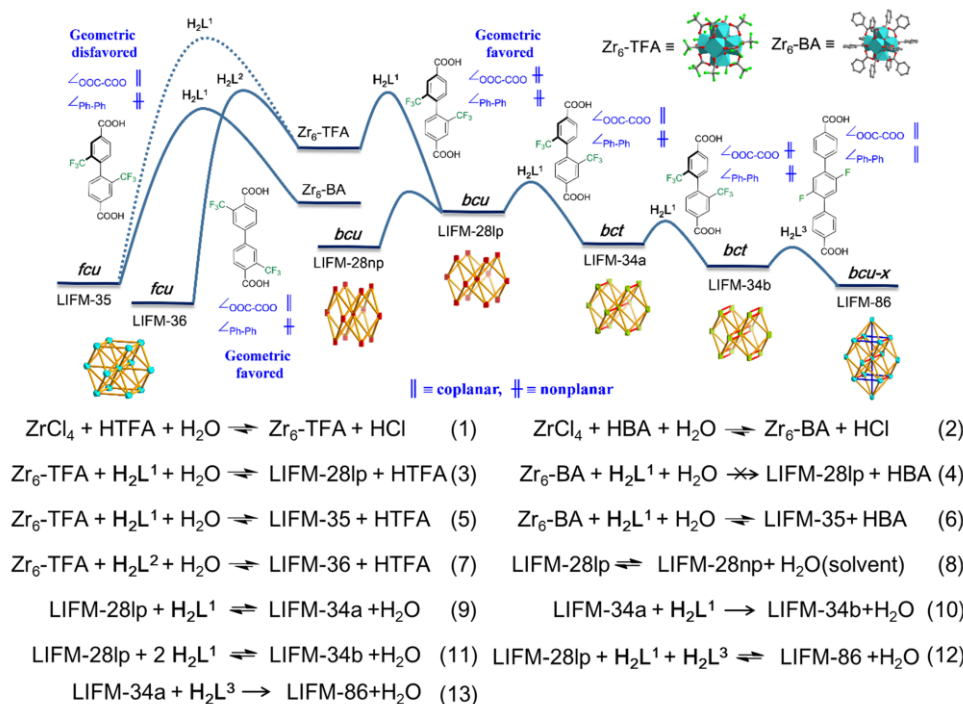


**Figure 5.** Synthetic map of obtained Zr-MOFs and proposed reactions (the reactions are not balanced and only main reactants are presented).

stability (Figures S23-S29). In general, the increased Zr<sub>6</sub>-cluster connectivity strengthens the framework and leads to higher decomposing temperature above 300 °C than that of LIFM-28. LIFM-28lp transforms to LIFM-28np at 100 °C, and then maintains the framework integrity up to 200 °C.<sup>[12]</sup> After insertion of H<sub>2</sub>L<sup>1</sup> and H<sub>2</sub>L<sup>3</sup> spacers, the framework stability increases up to 380 °C for LIFM-34a, 400 °C for LIFM-34b and 440 °C for LIFM-86 as confirmed by VT-PXRD measurements. LIFM-36 is thermally stable up to 360 °C; however, the isostructural LIFM-35 keeps its crystallinity only to 100 °C, which is consistent with the fact that LIFM-35 has highly constrained conformation of H<sub>2</sub>L<sup>1</sup> as linkers.

The chemical stability was evaluated by treating the samples with organic solvents and aqueous solutions at different pH values (Figures S30-S37). LIFM-28lp shows good stability in various organic solvents, and insertion of additional linkers even improves chemical stability in organic solvent with samples remaining intact after soaking for 10 days (exemplified by LIFM-34a/b). The thermodynamic product LIFM-36 displays excellent acid and base stability in aqueous solution with pH = 1 and 12, while the counterpart LIFM-35 collapses under similar conditions, following the same trend as its thermal stability. The kinetic product LIFM-28lp also shows high acid, base and water stability.<sup>[12]</sup> However, the labile spacer coordination makes LIFM-34a/34b/86 convert back to LIFM-28lp after soaking in water.

**Tuning of porosity and hydrophobicity.** N<sub>2</sub> adsorption performed on the activated samples of all Zr-MOFs show fully reversible type-I isotherms, characteristic of microporous materials (Figures S38-S45 and Table S6). The pore size distribution (PSD) analyses disclose that 8- and 10-connecting LIFM-28np/34a/34b have resembling pore distribution in the

range of 11-13 Å, while 12-connecting LIFM-35/36/86 show a pore dimension with diameters *ac.* 12 Å, which are consistent with their single-crystal structures. The apparent BET surface area and associated total pore volume of 8-connecting LIFM-28np are relatively low. Upon insertion of different linkers, these values are variably increased, approaching the highest ones in 12-connecting LIFM-35/36. Therefore, the varied framework topologies and pore surfaces decorated with different amount and type of F-atoms are expected to show impact on gas adsorption and separation properties.

On the other hand, insertion of additional linkers carrying on -CF<sub>3</sub> groups results in prominent hydrophobicity of the Zr-MOF pores. As seen from water vapor isotherms in Figure S46, the adsorption take-off points varied in different Zr-MOFs, which reflecting their hydrophobicity. A positive relation of hydrophobicity to the fluorine density insidepores is observed, *i.e.*, LIFM-36 > LIFM-34b > LIFM-34a > LIFM-28np. The PXRD patterns recorded after water uptake indicate that Zr-MOFs containing inserted linkers are transformed back to LIFM-28lp, revealing removal of inserted linkers that starts from their take-off points as verified by monitoring the phase change at different relative pressures in the water adsorption processes (Figures S47-S52). This also accounts for the poor hydrophobicity of LIFM-35 and LIFM-86, which are water unstable due to the presence of the constrained H<sub>2</sub>L<sup>1</sup> linkers. In comparison to the lowest hydrophobicity of LIFM-28np, LIFM-36 shows the more pronounced hydrophobicity and highest water uptake capacity, attributable to its highest F-density and effective shielding of hydrophilic Zr<sub>6</sub>-cluster by -CF<sub>3</sub> groups.

**Gas adsorption and separation selectivity.** The adsorption isotherms of R22, CO<sub>2</sub>, CH<sub>4</sub> and N<sub>2</sub> under different temperatures

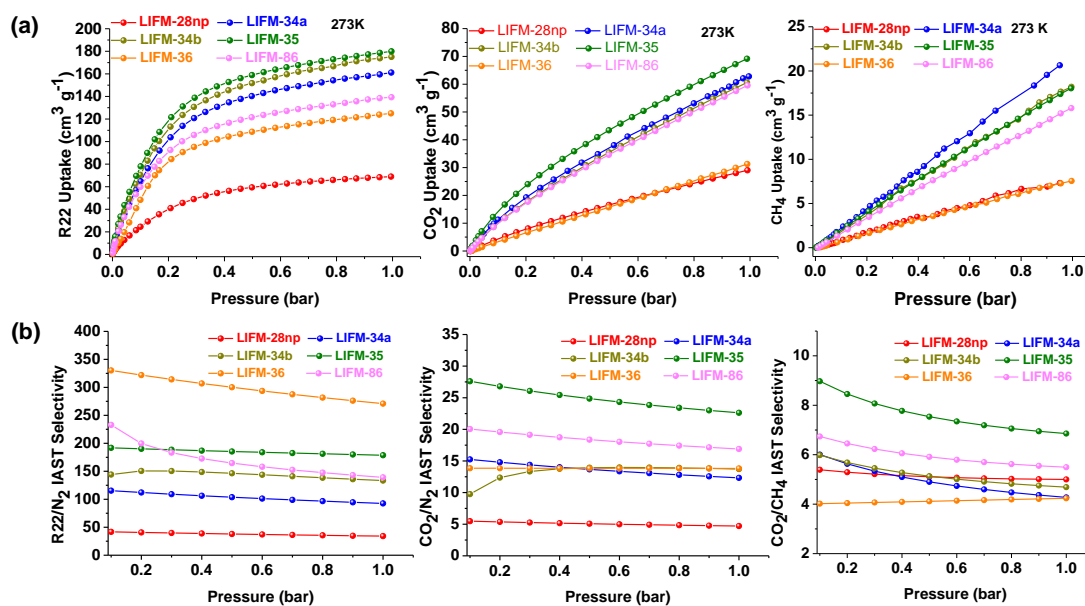


**Figure 6.** (a) R22, CO<sub>2</sub> and CH<sub>4</sub> sorption isotherms of Zr-MOFs at 273. (b) IAST calculated selectivity of R22/N<sub>2</sub> (10:90), CO<sub>2</sub>/N<sub>2</sub> (15:85) and CO<sub>2</sub>/CH<sub>4</sub>(50:50) at 273 K.

were measured, from which the adsorption enthalpies ( $Q_{st}$ ) of R22 and CO<sub>2</sub> and selectivities based on ideal adsorbed solution theory (IAST) for R22/N<sub>2</sub> (10:90), CO<sub>2</sub>/N<sub>2</sub> (15:85) and CO<sub>2</sub>/CH<sub>4</sub> (50:50) were calculated to estimate the promises of these materials for gas separation (Figures S53-S69). As seen from Figure 6, it is clear that the R22, CO<sub>2</sub> and CH<sub>4</sub> uptake capacity are not simply correlated with the pore volume. Indeed, LIFM-28 with much small pore volume has the lowest gas uptake capacity of R22, CO<sub>2</sub> and CH<sub>4</sub>, however the adsorption properties could be finely tuned in other diversified Zr-MOFs. The adsorbed R22 amounts are positively related to the F-density except for LIFM-36, showing a sequence of LIFM-35 > LIFM-34b > LIFM-34a > LIFM-86 > LIFM-36. This observation may be explained by the gradually increased pore volumes and intermolecular interactions between R22 and F-atoms on the framework, of which -CF<sub>3</sub> seems more effective than -F groups. The relatively lower R22 uptake by LIFM-36 suggests that -CF<sub>3</sub> groups far away from the middle of aromatic rings could not efficiently interact with R22 adsorbates. Similarly, LIFM-35 displays the best adsorption behavior toward CO<sub>2</sub> and CH<sub>4</sub>, in contrast to LIFM-36 with lowest uptake capacity, while the inserted linkers just cause adsorption increase without significant distinction, implying that interactions between F-atoms and CO<sub>2</sub>/CH<sub>4</sub> might be not as strong as those between carboxylate and CO<sub>2</sub>/CH<sub>4</sub>.

The strength of the host/guest interactions can be evaluated by the isosteric adsorption enthalpies ( $Q_{st}$ ) at low coverage calculated using the Clausius-Clapeyron equation applied to adsorption isotherms collected at different temperatures<sup>[26]</sup> (Figure S64). At initial adsorption, LIFM-34a/34b/35 show much higher  $Q_{st}$  than LIFM-28np/36, indicating prominent R22...CF<sub>3</sub> interactions if -CF<sub>3</sub> is located in proper positions. It is worthy of noting that  $Q_{st}$  values of LIFM-28np/36 are comparable with activated carbon (22.0-28.0 kJ mol<sup>-1</sup>),<sup>[27]</sup> while those of other Zr-

MOFs (30.4~36.4 kJ mol<sup>-1</sup>) are close to the highest energetic values reported, such as MIL-101 (34.6 kJ mol<sup>-1</sup>)<sup>[28]</sup>, MAF-X10 (32.9 kJ mol<sup>-1</sup>).<sup>[29]</sup> On the other hand, the  $Q_{st}$  of LIFM-36 is much lower than that of LIFM-28np, suggesting that protection of carboxylate by -CF<sub>3</sub> groups may alter effective interaction between CO<sub>2</sub> and carboxylate (Figure S64). It is found that LIFM-35 outperforms other Zr-MOFs in IAST selectivity of CO<sub>2</sub>/N<sub>2</sub> and CO<sub>2</sub>/CH<sub>4</sub>,<sup>[12, 15b]</sup> while LIFM-36 surpasses others in IAST selectivity of R22/N<sub>2</sub>.<sup>[12, 15b]</sup> The gas separation selectivities can be elaborately tuned based on a balance of F-density and distribution, as well as pore volume and size, which are determined by the distinct framework topologies and inserted linkers carrying on distinctively functionalized groups (Figure 6).

## Conclusion

In summary, by means of designing ligand conformations, controlling reaction temperature, choosing modulators, tuning reactant concentrations, applying post-synthetic spacer insertions, seven fluorinated Zr-MOFs have been obtained with two linear dicarboxylate ligands. The dynamic nature of Zr-O bond has been understood to gain an insight into the control factors determinate thermodynamic and kinetic Zr-MOF products, providing a useful platform for the structural tuning and transformation with post-modification and functionalization. Various influencing factors in synthesis and transformation processes have been explored and further elucidated by DFT calculations. Fine-tuning of Zr-MOF properties have been testified by thermal and chemical stability, hydrophobicity, gas uptake capacity and separation ability, establishing a rational structure-property relationship. This work not only provides a fundamental understanding of Zr-MOF dynamic chemistry, but also an endeavor to enrich synthetic chemistry of Zr-MOF for

structural control, tuning and functionalization beyond *de novo* synthesis.

## Acknowledgements

We are grateful for financial support by the NSFC (21821003, 21720102007, 21890380), the LIRT Project of GPRTP (2017BT01C161), Chinese Postdoctoral Science Fund (2017M622866), the International Postdoctoral Exchange Fellowship Program (20180055), and the FRF for the Central Universities.

**Keywords:** metal-organic frameworks•dynamics•post-synthesis•fluorine

- [1] Y. He, W. Zhou, G. Qian, B. Chen, *Chem. Soc. Rev.* **2014**, *43*, 5657-5678.
- [2] K. Adil, Y. Belmabkhout, R. S. Pillai, A. Cadiau, P. M. Bhatt, A. H. Assen, G. Maurin, M. Eddaoudi, *Chem. Soc. Rev.* **2017**, *46*, 3402-3430.
- [3] J. Liu, L. Chen, H. Cui, J. Zhang, L. Zhang, C. Y. Su, *Chem. Soc. Rev.* **2014**, *43*, 6011-6061.
- [4] (a) M. Ding, R. W. Flaig, H.-L. Jiang, O. M. Yaghi, *Chem. Soc. Rev.* **2019**, *48*, 2783-2828; (b) S. Furukawa, J. Reboul, S. Diring, K. Sumida, S. Kitagawa, *Chem. Soc. Rev.* **2014**, *43*, 5700-5734; (c) V. Guillermin, D. Kim, J. F. Eubank, R. Luebke, X. Liu, K. Adil, M. S. Lah, M. Eddaoudi, *Chem. Soc. Rev.* **2014**, *43*, 6141-6172; (d) H.-C. Zhou, J. R. Long, O. M. Yaghi, *Chem. Rev.* **2012**, *112*, 673-674.
- [5] (a) Y. Bai, Y. Dou, L.-H. Xie, W. Rutledge, J.-R. Li, H.-C. Zhou, *Chem. Soc. Rev.* **2016**, *45*, 2327-2367; (b) S. Wang, M. Wahiduzzaman, L. Davis, A. Tissot, W. Shepard, J. Marrot, C. Martineau-Corcoc, D. Hamdane, G. Maurin, S. Devautour-Vinot, C. Serre, *Nat. Commun.* **2018**, *9*, 4937; (c) S. Wang, J. S. Lee, M. Wahiduzzaman, J. Park, M. Muschi, C. Martineau-Corcoc, A. Tissot, K. H. Cho, J. Marrot, W. Shepard, G. Maurin, J.-S. Chang, C. Serre, *Nature Energy* **2018**, *3*, 985-993.
- [6] (a) Q. Sun, B. Aguila, J. A. Perman, T. Butts, F.-S. Xiao, S. Ma, *Chem* **2018**, *4*, 1726-1739; (b) C. Yang, U. Kaipa, Q. Z. Mather, X. Wang, V. Nesterov, A. F. Venero, M. A. Omary, *J. Am. Chem. Soc.* **2011**, *133*, 18094-18097; (c) T.-H. Chen, I. Popov, W. Kaveevivitchai, Y.-C. Chuang, Y.-S. Chen, A. J. Jacobson, O. S. Miljanic, *Angew. Chem. Int. Ed.* **2015**, *54*, 13902-13906.
- [7] (a) K. Lu, C. He, W. Lin, *J. Am. Chem. Soc.* **2015**, *137*, 7600-7603; (b) P. Deria, Y. G. Chung, R. Q. Snurr, J. T. Hupp, O. K. Farha, *Chem. Sci.* **2015**, *6*, 5172-5176.
- [8] (a) *Handbook of Fluorous Chemistry*, 1st ed., Wiley-VCH, Weinheim, Germany, **2004**; (b) M. Braitsch, H. Kahlig, G. Kontaxis, M. Fischer, T. Kawada, R. Konrat, W. Schmid, *Beilstein J. Org. Chem.* **2012**, *8*, 448-455; (c) M. Pagliaro, R. Ciriminna, *J. Mater. Chem.* **2005**, *15*, 4981-4991.
- [9] C.-Y. Su, A. M. Goforth, M. D. Smith, P. J. Pellechia, H.-C. zur Loye, *J. Am. Chem. Soc.* **2004**, *126*, 3576-3586.
- [10] L. Chen, J.-W. Ye, H.-P. Wang, M. Pan, S.-Y. Yin, Z.-W. Wei, L.-Y. Zhang, K. Wu, Y.-N. Fan, C.-Y. Su, *Nat. Commun.* **2017**, *8*, 15985-15994.
- [11] Q.-f. Qiu, C.-X. Chen, Z.-W. Wei, C.-C. Cao, N.-X. Zhu, H.-P. Wang, D. Wang, J.-J. Jiang, C.-Y. Su, *Inorg. Chim. Acta* **2019**, *58*, 61-64.
- [12] C.-X. Chen, Z. Wei, J.-J. Jiang, Y.-Z. Fan, S.-P. Zheng, C.-C. Cao, Y.-H. Li, D. Fenske, C.-Y. Su, *Angew. Chem. Int. Ed.* **2016**, *55*, 9932-9936.
- [13] C.-X. Chen, Z.-W. Wei, Q.-F. Qiu, Y.-Z. Fan, C.-C. Cao, H.-P. Wang, J.-J. Jiang, D. Fenske, C.-Y. Su, *Cryst. Growth Des.* **2017**, *17*, 1476-1479.
- [14] (a) R. E. Morris, L. Brammer, *Chem. Soc. Rev.* **2017**, *46*, 5444-5462; (b) P. Cui, P. Wang, Y. Zhao, W.-Y. Sun, *Cryst. Growth Des.* **2019**, *19*, 1454-1470.
- [15] (a) S. Yuan, W. Lu, Y.-P. Chen, Q. Zhang, T.-F. Liu, D. Feng, X. Wang, J. Qin, H.-C. Zhou, *J. Am. Chem. Soc.* **2015**, *137*, 3177-3180; (b) C.-X. Chen, Z.-W. Wei, J.-J. Jiang, S.-P. Zheng, H.-P. Wang, Q.-F. Qiu, C.-C. Cao, D. Fenske, C.-Y. Su, *J. Am. Chem. Soc.* **2017**, *139*, 6034-6037.
- [16] S. Yuan, J.-S. Qin, L. Zou, Y.-P. Chen, X. Wang, Q. Zhang, H.-C. Zhou, *J. Am. Chem. Soc.* **2016**, *138*, 6636-6642.
- [17] M. Vandichel, J. Hajek, A. Ghysels, A. De Vos, M. Waroquier, V. Van Speybroeck, *CrystEngComm* **2016**, *18*, 7056-7069.
- [18] C.-C. Cao, C.-X. Chen, Z.-W. Wei, Q.-F. Qiu, N.-X. Zhu, Y.-Y. Xiong, J.-J. Jiang, D.-W. Wang, C.-Y. Su, *J. Am. Chem. Soc.* **2019**, *141*, 2589-2593.
- [19] (a) T. Islamoglu, S. Goswami, Z. Li, A. J. Howarth, O. K. Farha, J. T. Hupp, *Acc. Chem. Res.* **2017**, *50*, 805-813; (b) M. Bosch, S. Yuan, W. Rutledge, H.-C. Zhou, *Acc. Chem. Res.* **2017**, *50*, 857-865; (c) S. M. Cohen, *Chem. Rev.* **2012**, *112*, 970-1000.
- [20] C.-X. Chen, Q.-F. Qiu, M. Pan, C.-C. Cao, N.-X. Zhu, H.-P. Wang, J.-J. Jiang, Z.-W. Wei, C.-Y. Su, *Chem. Commun.* **2018**, *54*, 13666-13669.
- [21] J. H. Cavka, S. Jakobsen, U. Olsbye, N. Guillou, C. Lamberti, S. Bordiga, K. P. Lillerud, *J. Am. Chem. Soc.* **2008**, *130*, 13850-13851.
- [22] S. Yuan, Y.-P. Chen, J.-S. Qin, W. Lu, L. Zou, Q. Zhang, X. Wang, X. Sun, H.-C. Zhou, *J. Am. Chem. Soc.* **2016**, *138*, 8912-8919.
- [23] (a) V. Bon, V. Senkovskyy, I. Senkovska, S. Kaskel, *Chem. Commun.* **2012**, *48*, 8407-8409; (b) V. Bon, I. Senkovska, M. S. Weiss, S. Kaskel, *CrystEngComm* **2013**, *15*, 9572-9577.
- [24] (a) M. J. Frisch, G. W. Trucks, H. B. Schlegel, G. E. Scuseria, M. A. Robb, J. R. Cheeseman, G. B. Scalmani, V.; B. Mennucci, G. A. Petersson, H. Nakatsuji, M. L. Caricato, X.; H. P. Hratchian, A. F. Izmaylov, J. Bloino, G. L. Zheng, J. L. Sonnenberg, M. E. Hada, M.; K. Toyota, R. Fukuda, J. Hasegawa, M. Ishida, T. Nakajima, Y. Honda, O. Kitao, H. Nakai, T. Vreven, J. A. Montgomery, J. E. Jr.; Peralta, F. Ogliaro, M. Bearpark, J. J. Heyd, E. Brothers, K. N. Kudin, V. N. Staroverov, T. Keith, R. Kobayashi, J. Normand, K. Raghavachari, A. Rendell, J. C. Burant, S. S. Iyengar, J. Tomasi, M. Cossi, N. Rega, J. M. Millam, M. Klene, J. E. Knox, J. B. Cross, V. Bakken, C. Adamo, J. Jaramillo, R. Gomperts, R. E. Stratmann, O. Yazyev, A. J. Austin, R. Cammi, C. Pomelli, J. W. Ochterski, R. L. Martin, K. Morokuma, V. G. Zakrzewski, G. A. Voth, P. Salvador, J. J. Dannenberg, S. Dapprich, A. D. Daniels, O. Farkas, J. B. Foresman, J. V. Ortiz, J. Cioslowski, D. J. Fox, *Gaussian, Inc.: Wallingford CT* **2010**; (b) R. Dennington, T. Keith, J. Millam, S. Inc., *Shawnee Mission, KS* **2009**.
- [25] (a) Guido Kickelbick, Petra Wiede, U. Schubert, *Inorg. Chim. Acta* **1999**, *284*, 1-7; (b) M. Puchberger, F. R. Kogler, M. Jupa, S. Gross, H. Fric, G. Kickelbick, U. Schubert, *Eur. J. Inorg. Chem.* **2006**, *2006*, 3283-3293; (c) C. Hennig, S. Weiss, W. Kraus, J. Kretzschmar, A. C. Scheinost, *Inorg. Chem.* **2017**, *56*, 2473-2480; (d) A. A. Bezrukov, K. W. Tomroos, E. Le Roux, P. D. C. Dietzel, *Chem Commun (Camb)* **2018**, *54*, 2735-2738; (e) Q. Sun, C. Liu, G. Zhang, J. Zhang, C. H. Tung, Y. Wang, *Chemistry* **2018**, *24*, 14701-14706; (f) C. C. Chiu, F. K. Shieh, H. G. Tsai, *Inorg. Chem.* **2019**, *58*, 14457-14466.
- [26] L. Czepirski, J. JagieŁo, *Chemical Engineering Science* **1989**, *44*, 797-801.
- [27] B. B. Saha, K. Habib, I. I. El-Sharkawy, S. Koyama, *Int. J. Refrig.* **2009**, *32*, 1563-1569.
- [28] R. K. Motkuri, H. V. Annapureddy, M. Vijaykumar, H. T. Schaefer, P. F. Martin, B. P. McGrail, L. X. Dang, R. Krishna, P. K. Thallapally, *Nat. Commun.* **2014**, *5*, 4368-4373.
- [29] R.-B. Lin, T.-Y. Li, H.-L. Zhou, C.-T. He, J.-P. Zhang, X.-M. Chen, *Chem. Sci.* **2015**, *6*, 2516-2521.

## Entry for the Table of Contents

The unusual coordination dynamics of seven fluorinated Zr-MOFs were explored by designing two trifluoromethyl functionalized ligands. Comprehensive factors for controllable syntheses and transformations have been discussed. The stability, hydrophobicity, and gas adsorption selectivities have been studied to elucidate the structure-property relationship. This work demonstrate that dynamic Zr-MOFs can be a versatile platform for functionalization.



Cheng-Xia Chen, Yan-Zhong Fan, Chen-Chen Cao, Hai-Ping Wang, Ya-Nan Fan, Ji-Jun Jiang, Zhang-Wen Wei\*, Guillaume Maurin\*, and Cheng-Yong Su\*

**Dynamic Coordination Chemistry of Fluorinated Zr-MOFs: Synthetic Control and Reassembly/Disassembly beyond *de novo* Synthesis to Tune the Structure and Property**

Accepted Manuscript